https://doi.org/10.5194/acp-2019-790
Preprint. Discussion started: 7 October 2019

Atmospheric Chemistry and Physics Discussions

Ceilometers as planetary boundary layer detectors and a corrective tool for ECMWF and COSMO NWP models

Leenes Uzan[1,2], Smadar Egert[1], Pavel Khain[2], Yoav Levi[2], Elyakom Vladislavsky[2], Pinhas Alpert[1]

[1] Department of Geosciences, Raymond and Beverly Sackler Faculty of Exact Sciences, Tel-Aviv University, Tel Aviv, 6997801, Israel.
[2] The Israeli Meteorological Service, Beit Dagan, Israel.

Correspondence to: Leenes Uzan (Leenesu@gmail.com)

Abstract

The growing importance of the planetary boundary layer (PBL) height detection is apparent in various fields, from air pollution analysis to weather prediction. In recent years micro-lidars such as ceilometers have been recognized as an efficient tool for such measurements. Here, the daytime summer PBL height is measured by eight ceilometers throughout Israel, along with radiosonde profiles, the global IFS model, and the regional COSMO model. The analysis focused on three PBL height evaluation methods: the bulk Richardson method, the parcel method, and the wavelet covariance transform method. The best agreement between the PBL heights derived from a single radiosonde site on 33 summer days was found by the adjacent ceilometer (mean error = 12 m, RMSE = 97 m). Spatial analysis of the PBL heights derived from the models on 13 days in reference to five ceilometer measurement sites revealed COSMO evaluations by the bulk Richardson method ($COSMO_R$) produced the best results for both flat (mean error = 19 m, RMSE = 203 m) and elevated terrain (mean error = -6 m, RMSE = 251 m). To improve $COSMO_R$ results, a regression tool was assimilated based on the PBL height difference between $COSMO_R$ and ceilometers. The regression is based on the altitude and distance from the shoreline for eight ceilometer sites.

https://doi.org/10.5194/acp-2019-790
Preprint. Discussion started: 7 October 2019

Atmospheric Chemistry and Physics Discussions

1. Introduction

In this era of heavy industrialization, the need to mitigate the detrimental effects of air pollution exposure is unquestionable. However, in order to regulate and establish environmental thresholds, a comprehensive understanding of the air pollution dispersion processes is necessary. One of the key meteorological parameters governing air pollution dispersion is the planetary boundary layer (PBL) height. The PBL is classified as the first level of the atmosphere which dictates the vertical dispersion extent of air pollution (Stull 1988). Consequently, the concentration level of air pollution varies depending on the height of the PBL.

Previous studies have successfully utilized ceilometers as a means to recognize and determine the PBL height (Eresmaa et al., 2006, Haeffelin and Angelini, 2012, Wiegner et al., 2014, Kotthaus and Grimmond, 2018). Over the past decade, however, the ceilometer has become recognized as a significant remote sensing tool, and is no longer perceived merely as a cloud base height detector (Wiegner et al., 2014). Ubiquitous in airports worldwide, ceilometers are valuable and effective instruments which produce high resolution aerosol backscatter profiles (every 15 s, every 10 m, up to several km). These qualities reflect their advantages over sophisticated lidars, which are limited in amount and operational time (Mamouri et al., 2016).

Gierens et al (2018) established a PBL height algorithm applied to the ceilometers' profiles. The PBL was classified according to daytime convective mixing and a nighttime stable surface layer accompanied by a residual layer aloft. Their research, conducted in northwestern South Africa during October 2012–August 2014, showed good agreement with ERA-Interim reanalysis.

Another operational PBL height detection method was established by Collaud Coen et al. (2014). Their study, implemented on a two-year data set for two rural sites located on the Swiss plateau, included several remote sensing instruments (wind profiler, Raman lidar, microwave radiometer) and several algorithms (the parcel method, the bulk Richardson number method, surface-based temperature inversion, aerosol or humidity gradient analysis). The results were validated against radio-sounding measurements and compared to the numerical weather prediction (NWP) model COSMO-2 (2.2 km resolution). The authors recommended using ceilometers for complementary measurement data of the residual layer alone.

Ketterer et al. (2014) focused on the development of the PBL in the Swiss Alps by an adjacent ceilometer, wind profiler, and in-situ continuous aerosol measurements. The ceilometer's

https://doi.org/10.5194/acp-2019-790
Preprint. Discussion started: 7 October 2019


Atmospheric Chemistry and Physics Discussions

profiles were analyzed by the gradient and STRAT-2D algorithms. Good agreement was found between the PBL height derived from the ceilometer and wind profiler during the daytime and under cloud-free conditions. However, comparisons to the calculated PBL heights from COSMO-2 model yielded low correlations.

Despite this extensive research, so far, scarce attention has been paid to designate ceilometers as a correction tool for NWP (Szintai and Kaufmann, 2007, Kuhn et al, 2018). In this study we analyze the daytime PBL height over complex terrain of Israel derived from NWP models and corrected by remote sensing measurements from eight ceilometers. Models and instruments are described in Sect. 3 and Sect. 4, respectively, and PBL height detection methods are presented in Sect. 5. The results of NWP models as compared to in-situ radiosonde and ceilometer measurements are presented in Sect. 6. Finally, conclusions are drawn in Sect. 7 regarding the capabilities of NWP models and the evolution of the daytime PBL height over Israel.

https://doi.org/10.5194/acp-2019-790
Preprint. Discussion started: 7 October 2019

Atmospheric Chemistry and Physics Discussions

2. Research area

Located in the East Mediterranean, Israel obtains systematic radiosonde atmospheric observations twice daily by the Israeli Meteorological Service (IMS) in Beit Dagan. Hence, the opportunity to widen the scope of atmospheric observation by means of affordable, low cost devices such as ceilometers is of utmost interest. This study was conducted using eight ceilometers deployed at diverse sites (Fig.1, Table 1), from the Mediterranean climate in north to the arid climate of the southern desert.

Essentially, as ceilometers produce aerosol backscatter profiles, evaluation of the PBL height during precipitation episodes becomes difficult (Collaud et al. 2014, Ketterer et al. 2014, Kotthaus & Grimmond 2018). Accordingly, in this study, we focused on the summer season, with no precipitation, high relative humidity (RH, up to 80% in midday in the shoreline, IMS weather reports), and sporadic shallow cumulous clouds. On the synoptic scale, the summer is characterized between June-September by a persistent Persian Trough (either deep, shallow or medium) followed by a Subtropical High aloft (Alpert et al., 2004). As a result, the average PBL height is comparatively low (~ 1000 m a.g.l).

Comprehensive research of the Israeli summer PBL (Neumann, 1952, Neumann, 1977, Dayan et al., 1988, Lieman, R. and Alpert, 1993, Hashmonay et al., 1991, Felix, 1993, Felix, 1994, Dayan and Rodnizki, 1999, Dayan et al., 2002, Alpert and Rabinovich-Hadar, 2003, Felix, 2004, Levi et al., 2011, Uzan and Alpert, 2012, Uzan et al 2016) is generally described in the following manner: After sunrise (~2-3 UTC) clouds initially formed over the Mediterranean Sea are advected eastward to the shoreline. As the ground warms up, the nocturnal surface boundary layer (SBL) dissipates and buoyancy induced convective updrafts instigate the formation of the sea breeze circulation. The entrance of sea breeze front (SBF) is estimated between 5-8 UTC, depending on the time of sunrise and the prevailing synoptic system. Cool and humid marine air hinder the convective updrafts, thus clouds dissolve and the height of the shoreline convective boundary layer (CBL) lowers by ~250 m. All the while, further inland, the convective thermals continue to inflate the CBL. Through the day, the sea breeze circulation steers clockwise and the wind speed is enhanced by the west-north-west synoptic winds. By noontime (~9-11 UTC) this combination achieves maximum wind speeds, suppressing the CBL even lower. Due to the large distance (~30-50 km inland), the SBF reaches the eastern elevated complex terrain only in the afternoon (~ 11-12 UTC). At sunset (~16-17 UTC), as the insolation diminishes, the potential energy of the convective updrafts weakens therefore the

https://doi.org/10.5194/acp-2019-790
Preprint. Discussion started: 7 October 2019


Atmospheric Chemistry and Physics Discussions

CBL height drops. After sunset, the CBL finally collapses and a residual layer (RL) is formed above a SBL. The combination of a typical summer low RL and increased humidity (due to ground cooling), produces a low condensation level which forms shallow evening clouds.

125

3. IFS and COSMO Models

The PBL short range forecasts were produced by two models used operationally by the IMS: the ECMWF (European Centre for Medium-range Weather Forecasts) Integrated Forecast
130 System (IFS) model and the regional COSMO (consortium for small-scale modelling) model (Table 2).

COSMO (~2.5km resolution) is based on the primitive thermo-hydrodynamic equations describing non-hydrostatic compressible flow in a moist atmosphere (Steppeler et al., 2003, Doms et al., 2011, Baldauf et al., 2011). Its vertical extension reaches 23.5 km (~30 hPa) with
135 60 vertical model levels. The model runs a two-time level integration scheme based on a third order of the Runge–Kutta method and a fifth-order of the upwind scheme for horizontal advection. Unlike IFS, the deep convection parametrization is switched off, while only the shallow convection is parametrized (Tiedtke, 1989). COSMO has been running at the IMS over the Eastern Mediterranean (EM) (domain 25-39 E/26-36 N) with the same resolution since
140 2013, with boundary and initial conditions from IFS. In 2015, the IFS horizontal resolution was ~13 km and 137 vertical levels. In 2016, the horizontal resolution was improved upon to reach ~10 km.

The resolution of all models influences their topography, causing the latter to vary from the real heights. Thus, in our research, which relied on the two aforementioned models, the PBL
145 heights were corrected to the actual ones above sea level (Table 1).

IFS profiles were limited to hourly resolution, while COSMO generated profiles every 15 minutes. To compare COSMO's PBL heights, a series of trials were performed to find the correct representation of hourly values as the last 15 minutes within an hour.

150

https://doi.org/10.5194/acp-2019-790
Preprint. Discussion started: 7 October 2019

Atmospheric Chemistry and Physics Discussions

4. Instruments

4.1 Ceilometers

Vaisala ceilometers type CL31 are commonly deployed worldwide, and are the main research tool in this study. CL31 is a pulsed, elastic micro-lidar, employing an Indium Gallium Arsenide (InGaAs) laser diode transmitter of near infrared (NIR) wavelength of 910 nm ±10 nm at 25˚C with a high pulse repetition rate of 10 kHz every two seconds (Vaisala ceilometer CL31 user's guide: http://www.vaisala.com). The backscatter signals are collected by an avalanche photodiode (APD) receiver and designed as attenuated backscatter profiles at intervals of 2-120 s (determined by the user).

Following Weigner et al., (2014), it should be noticed that as single wavelength lidars, ceilometers cannot produce any information on the microphysical properties of the atmospheric aerosol content. Therefore, the assessment of their optical depth is impossible. On the other hand, by employing a NIR wavelength, a pronounced change of the attenuated backscatter profile is mainly attributed to variations in the aerosol content, providing more reliable indications for clouds and atmospheric layers.

In this study, CL31 ceilometers were located in diverse sites (Fig.1), with the exception of ceilometer CL51, which was stationed in the Weizmann Institute. CL51 consists of a higher signal and signal-to-noise ratio, hence the backscatter profile measurement reaches up to 15.4 km. One drawback is that calibration procedures were nonexistent in all sites, and in most cases, maintenance procedures (cleaning of the ceilometer window) were not regularly carried out, with the exception of the IMS Beit Dagan ceilometer. However, the PBL detection algorithm utilized here (see Sect. 5.3) is based on a significant signal slope, therefore can be determined from uncalibrated ceilometers.

The diurnal PBL measured by the ceilometers is the CBL at daytime and RL at nighttime (Ketterer et al., 2014). In this research, the SBL was not investigated due to a constant perturbation within the first range gates at the overlap height between the emitted laser beam and the receiver's field of view. Detailed information regarding manufactural and technical properties of ceilometers involved in this research, are given in Uzan et al. (2018). To compare the hourly results of the models (Sect. 3), the ceilometers' 15 seconds profiles were averaged to half-hour ones, whereas the second half-hour profile within each hour was chosen.

https://doi.org/10.5194/acp-2019-790
Preprint. Discussion started: 7 October 2019

Atmospheric Chemistry and Physics Discussions

4.2 Radiosonde

Radiosonde (RS) type Vaisala RS41-SG is launched twice daily at 23 UTC and 11 UTC by the IMS in the Beit Dagan site, adjacent to the ceilometer. The radiosonde generates profiles of RH, temperature, and pressure, as well as wind speed and wind direction. The PBL height was determined by profiles retrieved every 10 seconds at ~ 45 m height resolution.

5. Methods

5.1 The bulk Richardson number method

Both COSMO and IFS calculate the PBL height using the bulk Richardson number method (R_b) as the most reliable technique for NWM PBL height detection (Zhang et al., 2014). The bulk Richardson number is an approximation of the gradient Richardson number, which anticipates thermal convection via thermal energy, despite the resistance of turbulent kinetic energy referred to as wind shear:

$$R_b = \frac{\frac{g}{T_v}\Delta\theta_v \Delta Z}{(\Delta U)^2+(\Delta V)^2} \quad (1)$$

where g is the gravitational force , T_v is the virtual temperature , $\Delta\theta_v$ is the difference in the virtual potential temperature along a vertical height of Δz , ΔU and ΔV is the difference in the horizontal wind speed components. Essentially, the bulk Richardson number is a dimensionless ratio between the two main forces in the troposphere, namely, buoyancy and wind shear.

The bulk Richardson number formula for a certain height (Hanna R. Steven ,1969, Zhang et al., 2014) is given in the following manner:

$$R_b = \frac{\frac{g}{\theta_v}(\theta_{vz}-\theta_{v0})(Z-Z_0)}{U^2+V^2} \quad (2)$$

where g is the gravitational force, θ_{vz} is the virtual potential temperature at height Z, θ_{v0} is the virtual potential temperature at ground level (Z_0) (hence equals the virtual temperature - T_v), U and V are the horizontal wind speed components at height Z.

https://doi.org/10.5194/acp-2019-790
Preprint. Discussion started: 7 October 2019


Atmospheric Chemistry and Physics Discussions

The IFS model defines the PBL height as the lowest level at which the bulk Richardson number (Eq. 2) reaches a critical threshold of 0.25 (ECMWF-IFS documentation – Cy43r3, Part IV: Physical Processes, July 2017). The PBL height is distinguished by scanning the bulk Richardson results from the surface upwards. When the PBL height is found between two levels of the model, it is determined by linear interpolation.

COSMO estimates the bulk Richardson number based on the dynamic conditions of the first four levels (10, 34.2, 67.9, 112.3 m a.g.l.) signified by 0.33 for stable conditions and 0.22 for unstable ones. If no level is found, then a missing value is assigned for the PBL height.

In this study, the hot and dry summer nights of the Israeli summer produce stable SBL described by values that are higher than the aforementioned thresholds. Such cases inhibit PBL detection by the bulk Richardson number method. Consequently, we focused on the daytime hours between 9-14 UTC when convective conditions prevail.

5.2 The parcel method

The PBL height defined by the parcel method (Holzworth 1964, Stull, 1988, Seidel et al., 2010) as the height aloft at which the value of the virtual potential temperature reaches the that of the surface level. The calculation of the virtual potential temperature is as follows:

$$\theta_v = T_v \left(\frac{P_0}{P}\right)^{\frac{Rd}{Cp}} \quad (3)$$

where P_0 is the ground level atmospheric pressure, P is the at atmospheric pressure at height Z, R_d is the gas constant of dry air, C_p is the heat capacity of dry air in a constant pressure ($\frac{R_d}{C_p}$ = 0.286).

The virtual temperature (T_v) is obtained by:

$$T_v = \frac{T}{1-\frac{e}{P}(1-\varepsilon)} \quad (4)$$

where T is the temperature at height Z, e is the actual vapor pressure and ε is the ratio of the gas constant of air and water vapor (ε=0.622). The actual pressure (e, Eq. (5)) is derived by the relative humidity (RH) profile. The saturated vapor pressure (e_s) is calculated by Eq. (6) based on the temperature profile.

https://doi.org/10.5194/acp-2019-790
Preprint. Discussion started: 7 October 2019


Atmospheric Chemistry and Physics Discussions

$$e = e_s \frac{RH}{100} \quad (5)$$

$$e_s = 610.78 \exp\left(\frac{T}{T+238.3} 17.2694\right) \quad (6)$$

The IFS model creates profiles of specific humidity instead of RH, hence, we calculated the actual vapor pressure (e), given in Eq. (5), by the following equation:

$$e = \frac{qP}{0.378q+\varepsilon} \quad (7)$$

where q is the specific humidity, P is the pressure at the height Z, and ε is the ratio of the gas constant of air and water vapor (ε=0.622).

5.3 The wavelet covariance transform method

In our study, ceilometer PBL height is detected by the backscatter profiles above the height of the overlap function (~ 100 m, see Sect. 2.1). When clouds are present (mainly summer shallow cumulous), the algorithm defines the top of the clouds, denoted as the height were the signal counts decrease to the amount retrieved by background values. The cloud top height is defined as the PBL height, signifying the height where the shallow convective cloud updrafts cease and the free atmosphere begins (Stull, 1988). If no clouds exist, the algorithm defines an upper limit as the lowest height among two categories: the point with the highest variance between consecutive steps (20 m resolution), or the first point with negative values corresponding to low signal-to-noise ratio. Finally, the wavelet covariance transform (WCT) method is operated along the backscatter profile within the aforementioned height limits.

The WCT method (Brooks Ian, 2003), based on the Haar step function (Baars et al., 2012, is given in Eq. (8) and Eq. (9) as follows:

$$W_{f(a,b)} = \frac{1}{a} \int_{Zb}^{Zt} f(z) h\left(\frac{z-b}{a}\right) dz \quad (8)$$

where $W_{f(a,b)}$ is the local maximum along the backscatter profile ($f(z)$), determined within step (a) defined by the number of height levels multiplied by the profiles height resolution ($a = n\,\Delta z$). The profile's lower (Zb) and upper (Zt) boundaries and the Haar step function given in Eq. (9).

https://doi.org/10.5194/acp-2019-790
Preprint. Discussion started: 7 October 2019

Atmospheric Chemistry and Physics Discussions

$$h\left(\frac{z-b}{a}\right) = \begin{cases} +1, & b - \frac{a}{2} \le z \le b, \\ -1, & b \le z \le b + \frac{a}{2} \\ 0, & elsewhere \end{cases} \quad (9)$$

The Haar function is equivalent to a derivative, representing the value difference of each step above and beneath the point of interest (b). On clear days, the highest derivative (local maximum) occurs at the transition zone between the CBL and the free atmosphere. When clouds do exist, the strongest gradients appear when light emitted by the ceilometer encounters the cloud aerosols, and the local maximum is indicated as the cloud base height. However, as previously mentioned, our algorithm denotes the PBL height as the top of the shallow cloud (Stull, 1988).

6. Results

6.1 Comparison to in-situ radiosonde profiles

Statistical analysis of the Beit Dagan PBL heights mean error (ME), root mean square error (RMSE), and correlation (R) is presented (Fig. 2, Table 3) at 11 UTC from radiosonde profiles, the Beit Dagan ceilometer, and the two models. The PBL heights were derived by the bulk Richardson method (denoted by subscript R) and the parcel method (denoted by subscript P). The analysis was carried out for 33 summer days (13 days from August 2015 and 20 from Aug 2016) available from all models and instruments. The PBL heights of the radiosonde obtained the same results by either method (RS_P, RS_R) and this was the base of comparison. The best agreement was found between the ceilometer and the radiosonde results (ME=12, RMSE=97, and R=0.93). A large gap (800 m) was found between IFS_R and the radiosonde's PBL on August 17, 2016 consisting of an uncommon multi-cloud layer. Consequently, the recorded imprecision could be due to fact that the Richardson method is based solely on dry thermodynamics for local turbulence (Von Engeln and Teixeira, 2013), while on August 17, 2016, the 11 UTC PBL height was determined through a multi-layer cloud formation (Fig.3). Nevertheless, COSMO results based on the parcel method ($COSMO_P$) managed to retain the radiosonde's PBL height despite cloud formation. Overall, the Beit Dagan ceilometer's estimations show the best results. Therefore, the PBL measured by five ceilometers (including

https://doi.org/10.5194/acp-2019-790
Preprint. Discussion started: 7 October 2019

Atmospheric Chemistry and Physics Discussions

290 Beit Dagan) will be used as a reference for the spatial analysis where radiosonde measurements are not performed.

6.2 Spatial analysis by ceilometers

In the next stage, the same analysis was carried out at 11 UTC; this time, however, instead of
295 focusing on only one location, it was performed on five ceilometer sites (Ramat David, Tel Aviv, Beit Dagan, Weizmann and Jerusalem). Yet, in order to include the Beit Dagan single radiosonde launching in the PBL height measurements under uniform meteorological conditions, we were limited to 13 dates. When we evaluated the models' grid points corresponding to the ceilometers' sites, we discovered both models defined Tel Aviv within a
300 grid point that was mostly over the Mediterranean Sea. Therefore, we shifted the Tel Aviv site to an adjacent grid representing the Tel Aviv site in the same height and distance from shoreline within a grid point that was mostly land.

Exploration of the spatial evolution of the PBL height was implemented on 13 specific days retaining data from all instruments and models. Figure 4 presents the PBL height over five
305 ceilometer sites representing diverse terrain. The comparison to the radiosonde's PBL heights revealed a significant case on August 10, 2015 where all models overestimated the PBL height. Inspection models and radiosonde virtual potential temperature profiles for August 10, 2015 (Fig. 5) showed that an additional layer aloft affected the overestimation of the models leading to the discrepancy.

310 Inspection of the IFS results by both methods (IFS_R, IFS_P) revealed the model's limited capacity to precisely represent the PBL heights of specific sites even over flat terrain. This is expressed by overestimations in Tel Aviv (5 m a.s.l) and Beit Dagan (33 m a.s.l) given as RMSEs of 276-568 (Table 4). On the one hand, lower RMSEs (173-278, Table 4) were calculated in Weizmann (60 m a.s.l) and Ramat David (50 m a.s.l) sites.

315 Largely, COSMO PBL height based on the bulk Richardson method ($COSMO_R$) achieved the best statistical results (Tables 4-5) regarding flat and complex terrain altogether.

https://doi.org/10.5194/acp-2019-790
Preprint. Discussion started: 7 October 2019


Atmospheric Chemistry and Physics Discussions

6.3 COSMO PBL height correction

Finally, we analyzed the spatial evolution of the PBL height over Israel based on $COSMO_R$. The COSMO model at 2.5 km resolution results were compared to the PBL heights discerned by eight ceilometer sites (Fig. 1, Table 1) for the daytime hours between 9 - 14 UTC (corresponding to 11 -16 LST). Correction of $COSMO_R$ results was made by means of a regression function implemented separately for each hour, for all sites simultaneously. The regression formula is as follows:

$$ME_{st} = \alpha G + \beta D + \gamma \quad (10)$$

where ME_{st} is the dependent variable representing the PBL height mean error for each ceilometer station (st) compared to the results obtained by the $COSMO_R$. The independent predictor variables are the ground altitude of the ceilometer's site (G) and its distance from the shoreline (D). The correction factors α, β and γ are implemented on the $COSMO_R$ PBL height results.

We must note that here, the mean error PBL height was based on all available dates for each site on August 2015, as detailed in the following figures. Figure 6 demonstrates the correction process for 14 UTC with a maximum correction of ~300 m over a complex terrain surrounding Jerusalem (830 m a.s.l) and Nevatim (400 m a.s.l). A summary of the correction results appears in Fig. 7. Apparently, this correction reduced the COSMO diurnal PBL height difference. As expected (see Sect. 2), at 9 UTC the PBL height is the highest over Tel Aviv and the lowest over Jerusalem. At 11 UTC, however, an opposite process occurs as the PBL height descends near the shore and ascends over mountainous Jerusalem. Finally, at 14 UTC, as the solar insolation decreases, Tel Aviv PBL height is ~200 m lower than evaluated for midday (9 UTC), slowly descending over Jerusalem as well.

7. Conclusions

Earlier studies have successfully employed ceilometers for PBL height detection, typically under dry conditions. However, these studies employed weather models primarily as a validation tool rather than investigating the models' predictive capabilities. Here, we tested the accuracy of PBL height estimations from two operational models, the IFS global model (~ 9 and ~16 km resolution) and the meso-scale COSMO regional model (~2.5 km resolution). The

https://doi.org/10.5194/acp-2019-790
Preprint. Discussion started: 7 October 2019


Atmospheric Chemistry and Physics Discussions

models calculate the PBL height by the bulk Richardson method. Therefore, the PBL height estimations were relevant to daytime convection, which focused upon 11 UTC in our study. The radiosonde and models' results were generated by the bulk Richardson method and the parcel method as well. The results were compared to the ceilometers' PBL heights in August 2015 and 2016 detected by the WCT method.

We found the best correlation (0.91) and lowest RMSE (109 m) between the radiosonde's heights and the adjacent Beit Dagan ceilometer. Comparison of the models' PBL heights to the ceilometers' heights in four additional sites without radiosonde measurements, it was found that COSMO based on the bulk Richardson method ($COSMO_R$) achieved the most in both flat and elevated terrain. Apparently, IFS overestimated the evolution of the PBL height as it progressed inland to the elevated Jerusalem site (830 m a.s.l).

The combination of ceilometers and a high resolution COSMO model enabled us to generate, for the first time, a corrected spatial evolution of the daytime PBL (9-14 UTC) height over Israel.

Despite the limited database, our results offer a preview of the great potential of ceilometers as a correction tool to discern PBL height derived from weather models. Future research should therefore include a larger dataset to evaluate whether these results are retained in the long term and to define a systematic validation process.

https://doi.org/10.5194/acp-2019-790
Preprint. Discussion started: 7 October 2019

Atmospheric Chemistry and Physics Discussions

Data availability

Weather reports- Israeli Meteorological Service weather reports (in Hebrew): http://www.ims.gov.il/IMS/CLIMATE/ClimateSummary.

Radiosonde profiles – Israeli Meteorological Service provided by request.

Ceilometer profiles - the data is owned by governmental offices. The data is not online and provided by request.

Author contribution

Leenes Uzan carried out the research and prepared the manuscript under the careful guidance of Pinhas Alpert and Smadar Egert alongside a fruitful collaboration with Yoav Levi, Pavel Khain and Elyakom Vladislavsky. The authors declare that they have no conflict of interest.

Acknowledgements

We wish to thank the Israeli Meteorological Service, the Israeli Air Force, the Association of Towns for Environmental Protection (Sharon-Carmel), and Rafat Qubaj from the Department of Earth and Planetary Sciences at the Weizmann Institute of Science, for their ceilometer data. We are indebted to Hadas Marcus for her editing assistance.

https://doi.org/10.5194/acp-2019-790
Preprint. Discussion started: 7 October 2019

Atmospheric Chemistry and Physics Discussions

References

Alpert P., and Rabinovich-Hadar M.: Pre- and post-frontal lines - A meso gamma scale analysis over south Israel, J. Atmos. Sci., 60, 2994-3008, 2003.

Alpert, P., Osetinsky, I., Ziv, B., Shafir H.: Semi-objective classification for daily synoptic systems: Application to the eastern Mediterranean climate change. Int. J. of Climatol., 24, 1001-1011, 2004.

Baars, H., Ansmann, A., Engelmann, R., and Althausen, D.: Continuous monitoring of the boundary layer top with lidar, Atmos. Chem. Phys., 8, 7281–7296, https:// doi:10.5194/acp-8-7281-2008, 2008.

Baldauf, M., A. Seifert, J. Förstner, D. Majewski, M. Raschendorfer, and T. Reinhardt: Operational Convective-Scale Numerical Weather Prediction with the COSMO Model: Description and Sensitivities. Mon. Wea. Rev., 139, 3887–3905, https://doi.org/10.1175/MWR-D-10-05013.1, 2001.

Bechtold, P.: Convection parametrization. ECMWF Seminar proceedings on "The parametrization of subgrid physical processes", 63-85, 2008.

Brooks, I.: Finding Boundary Layer Top: Application of a wavelet covariance transform to lidar backscatter profiles, J. Atmos. Ocean. Tech., 20, 1092–1105, 2003.

Collaud Coen, M., Praz, C., Haefele, A., Ruffieux, D., Kaufmann, P., and Calpini, B.: Determination and climatology of the planetary boundary layer height above the Swiss plateau by in situ and remote sensing measurements as well as by the COSMO-2 model, Atmos. Chem. Phys., 14, 13205-13221, https://doi.org/10.5194/acp-14-13205-2014, 2014.

Dayan, U., Shenhav, R., Graber, M.: The Spatial and temporal behavior of the mixed layer in Israel, J Appl Meteorol, 27, 1382- 1394, 1988.

Dayan, U., Rodnizki, J.: The temporal behavior of the atmospheric boundary layer in Israel. J Appl Meteorol, 38, 830-836, 1999.

Dayan, U., Lifshitz-Goldreich B., and Pick, K.: Spatial and structural variation of the atmospheric boundary layer during summer in Israel-Profiler and rawinsonde measurements. J. Appl. Meteor., 41, 447-457,2002.

https://doi.org/10.5194/acp-2019-790
Preprint. Discussion started: 7 October 2019

Doms, G., J. Förstner, E. Heise, H.-J. Herzog, D. Mironov, M. Raschendorfer, T. Reinhardt, B. Ritter, R. Schrodin, J.-P. Schulz, and G. Vogel: A description of the nonhydrostatic regional COSMO model. Part II: Physical parameterization. Deutscher Wetterdienst, Ofenbach, 154 pp, 2011.

Eresmaa, N., Karppinen, A., Joffre, S. M., Räsänen, J., and Talvitie, H.: Mixing height determination by ceilometer, Atmos. Chem. Phys., 6, 1485-1493, https://doi.org/10.5194/acp-6-1485-2006, 2006.

Feliks, Y.: A numerical model for estimation of the diurnal fluctuation of the inversion height due to a sea breeze, Bound. Layer Meteor., 62, 151-161. 1993.

Feliks, Y: An analytical model of the diurnal oscillation of the inversion base due to sea breeze, J. Atmos. Sci., 51, 991-998,1994.

Feliks, Y: Nonlinear dynamics and chaos in the sea and land breeze, J. Atmos. Sci., 61, 2169-2187, 2004.

Gierens, R.T., Henriksson, S., Josipovic, M., Vakkari, V., Van Zyl, P.G., Beukes J.P., Wood, C.R., O'Connor, E.J.: Observing continental boundary layer structure and evolution over the South African savannah using a ceilometer, Theor. Appl. Climatoi., 136, 333-346, https://doi.org/10.1007/s00704-018-2484-7, 2018.

Haeffelin, M. and Angelini, F.: Evaluation of mixing height retrievals from automatic profiling lidars and ceilometers in view of future integrated networks in Europe, Bound. Lay. Meteorol., 143, 49–75, 2012.

Hanna, S. R.: The thickness of the planetary boundary layer, Atmos. Environ., 3, 519–536, 1969.

Hashmonay, R., Cohen, A., and Dayan, U.: Lidar observations of the atmospheric boundary layer in Jerusalem, J. Appl. Meteorol, 30, 1228-1236, 1991.

Holzworth, C. G.: Estimates of mean maximum mixing depths in the contiguous United States, Mon. Weather Rev., 92, 235–242, 1964.

Ketterer, C., Zieger, P., Bukowiecki, N.: Bound. Lay. Meteo., 151, 317-334, https://doi.org/10.1007/s10546-013-9897-8, 2014.

https://doi.org/10.5194/acp-2019-790
Preprint. Discussion started: 7 October 2019

Atmospheric Chemistry and Physics Discussions

Kotthaus, S. and Grimmond, C.S.B.: Atmospheric boundary-layer characteristics from ceilometer measurements. Part 1: a new method to track mixed layer height and classify clouds, Q J R Meteorol. Soc.,144 (714), 1525–1538, https://doi.org/10.1002/qj.3299, 2018.

Kuhn, P., Wirtz, M., Killius, N., Wilbert, S., Bosch, J.L., Hanrieder, N., Nouri, B., Kleissle, J., Ramirez, L., Schroedter-Homscheidt, M., Heinemann, D., Kazantzidis, A., Blanc, P. and Pitz-Paal, R.: Benchmarking three low cost, low maintenance cloud height measurement systems and ECMWF cloud heights, Sol. Energy, 168, 140-152, https://doi.org/10.1016/j.solener.2018.02.050, 2018.

Levi Y., Shilo E., and Setter I.: Climatology of a summer coastal boundary layer with 1290-MHz wind profiler radar and a WRF simulation, J. Appl. Meteorol. Climatol., 50, 1815-1826, https://doi.org/10.1175/2011JAMC2598.1, 2011.

Lieman, R. and Alpert, P.: Investigation of the planetary boundary Layer height variations over complex terrain, Bound. Lay. Meteorol., 62, 129-142, 1993.

Mamouri, R.E., Ansmann, A., Nisantzi, A., Solomos, S., Kallos, G. and Hadjimitsis, D.G.: Extreme dust storm over the Eastern Mediterranean in September 2015: satellite, lidar, and surface observations in the Cyprus region, Atmos. Chem. Phys., 16(21), 13711-13724, 2016.

Neumann J.: Diurnal variations of the subsidence inversion and associated radio wave propagation phenomena over the coastal area of Israel. Isr. Met. Serv, 1952.

Neumann J.: On the rotation rate of direction of sea and land breezes. J. Atmos. Sci., 34, 1913-1917, 1977.

Szintai B., and Kaufmann P.: TKE as a measure of turbulence, Calibration of COSMO model, COSMO Newsletter No. 8, 2008.

Seidel, D. J., Ao, C. O., and Li, K.: Estimating climatological planetary boundary layer heights from radiosonde observations: Comparison of methods and uncertainty analysis, J. Geophys. Res., 115, D16113, doi:10.1029/2009JD013680, 2010.

Steppeler J., Doms G., Schattler U., Bitzer HW, Gassmann A., Damrath U., Gregoric G.: Meso gamma scale forecasts by nonhydrostatic model LM. Meteorological Atmospheric Physics, 82, 75–96, 2003.

Stull R.B.: An introduction to boundary layer meteorology, Kluwer Academic publishers, the Netherlands, 666 p., 1988.

https://doi.org/10.5194/acp-2019-790
Preprint. Discussion started: 7 October 2019

Atmospheric Chemistry and Physics Discussions

Tiedtke, M., 1989: A Comprehensive Mass Flux Scheme for Cumulus Parameterization in Large-Scale Models. Mon. Wea. Rev., 117, 1779–1800, https://doi.org/10.1175/1520-0493, 1989 .

Uzan, L. and Alpert, P.: The coastal boundary layer and air pollution - a high temporal resolution analysis in the East Mediterranean Coast, The Open Atmospheric Science Journal, 6, 9–18, 2012.

Uzan, L., Egert, S., and Alpert, P.: Ceilometer evaluation of the eastern Mediterranean summer boundary layer height – first study of two Israeli sites, Atmos. Meas. Tech., 9, 4387–4398, https://doi.org/10.5194/amt-9-4387-2016, 2016.

Von Engeln A., and Teixeira J.: A planetary boundary layer height climatology derived from ECMWF reanalysis data. J. Climate., 126, 6575-6590, https://doi.org/10.1175/JCLI-D-12-00385, 2013.

Wiegner M., Madonna F., Binietoglou I., Forkel R., Gasteiger J., Geiß A., Pappalardo G., Schäfer K., and Thomas W.: What is the benefit of ceilometers for aerosol remote sensing? An answer from EARLINET, Atmos. Meas. Tech., 7, 1979–1997, https://doi.org/10.5194/amt-7-1979-2014, 2014.

Zhang, Y., Gao, Z., Li, D., Li, Y., Zhang, N., Zhao, X., and Chen, J.: On the computation of planetary boundary-layer height using the bulk Richardson number method, Geosci. Model Dev., 7, 2599-2611, https://doi.org/10.5194/gmd-7-2599-2014, 2014.

https://doi.org/10.5194/acp-2019-790
Preprint. Discussion started: 7 October 2019

Atmospheric Chemistry and Physics Discussions

Table 1. Ceilometers parameters

Location	Site	Long/Lat	Distance from shoreline (km)	Height (m a.s.l)	Ceilometer type (resolution, height limit[a])
Ramat David (RD)	North	32.7 °/35.2 °	24	50	CL31 (10 m,16 s, up to 7.7 km)
Hadera (HD)	Shoreline	32.5 °/34.9 °	3.5	10	CL31 (10 m,16 s, up to 7.7 km)
Tel Aviv (TLV)	Shoreline	32.1 °/34.8 °	0.05	5	CL31 (10 m,16 s, up to 7.7 km)
Beit Dagan (BD)	Inland	32.0 °/34.8 °	7.5	33	CL31 (10 m,15 s, up to 7.7 km)
Weizmann (WZ)	Inland	31.9 °/34.8 °	11.5	60	CL51 (10 m,16 s, up to 15.4 km)
Jerusalem (JR)	Mountain	31.8 °/35.2 °	53	830	CL31 (10 m,16 s, up to 7.7 km)
Nevatim (NV)	South	31.2 °/34.9 °	44	400	CL31 (10 m,16 s, up to 7.7 km)
Hazerim (HZ)	South	31.2 °/34.7 °	70	200	CL31 (10 m,16 s, up to 7.7 km)

[a]The height limit depends on sky conditions and decreases as the atmospheric optical density (AOD) increases. Data acquisition was limited to 4.5 km by the ceilometers' software (BLview), except for in Beit Dagan.

Table 2. Characteristics of the NWP models

Model	Operation center	Resolution (deg)	Type	Convection parametrization
COSMO	IMS	0.025	Regional, boundary conditions from IFS	Mass flux Tiedtke shallow convection
IFS	ECMWF	0.1 in 2015 0.125 in 2016	Global	Mass flux Tiedke-Bechtold

https://doi.org/10.5194/acp-2019-790
Preprint. Discussion started: 7 October 2019

Atmospheric Chemistry and Physics Discussions

Table 3. Statistical analysis of the Beit Dagan PBL heights on 33 summer days (13 days in August 2015 and 20 days in August, 2016) from IFS and COSMO models by the bulk Richardson method (IFS_R, $COSMO_R$), the parcel method (IFS_P, $COSMO_P$) and the WCT method for the adjacent ceilometer. The PBL heights were compared to those derived from Beit Dagan radiosonde by either the parcel or bulk Richardson methods (same results, see Fig 2).

PBL detection	IFS_R	IFS_P	$COSMO_R$	$COSMO_P$	Ceilometer
Mean Error (m)	274	249	-3	-17	12
RMSE (m)	432	409	152	179	97
R	0.18	0.18	0.83	0.73	0.93
Mean PBL (m a.s.l)	1250	1225	973	959	989
Std PBL (m)	274	256	273	229	259

Table 4. Root mean square errors of PBL heights from five sites on 13 summer days (Fig. 4), derived by IFS and COSMO models by the bulk Richardson method (IFS_R, $COSMO_R$) and the parcel method (IFS_P, $COSMO_P$). The PBL heights were compared to the heights measured by Beit Dagan ceilometer.

Site	IFS_R	IFS_P	$COSMO_R$	$COSMO_P$
Ramat David	173 m	191 m	247 m	241 m
Tel Aviv	276 m	465 m	203 m	183 m
Beit Dagan	405 m	569 m	235 m	234 m
Weizmann	214 m	274 m	175 m	145 m
Jerusalem	351 m	368 m	251 m	273 m

Table 5. Same as in Table 3 but for mean errors.

Site	IFS_R	IFS_P	$COSMO_R$	$COSMO_P$
Ramat David	-31 m	30 m	-26 m	0 m
Tel Aviv	234 m	376 m	19 m	-35 m
Beit Dagan	332 m	497 m	12 m	-9 m
Weizmann	114 m	218 m	16 m	-42 m
Jerusalem	298 m	327 m	-6 m	29 m

https://doi.org/10.5194/acp-2019-790
Preprint. Discussion started: 7 October 2019

Atmospheric Chemistry and Physics Discussions

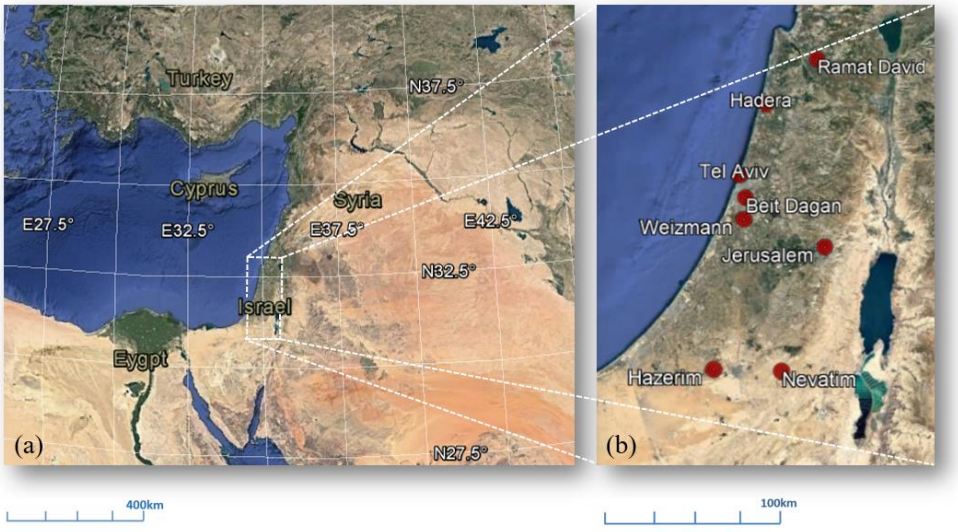

560 Fig. Maps of (a) the East Mediterranean and (b) the research area including indications of the ceilometers sites (red circles). Adapted from © Google Maps 2019.

565

570

https://doi.org/10.5194/acp-2019-790
Preprint. Discussion started: 7 October 2019

Atmospheric Chemistry and Physics Discussions

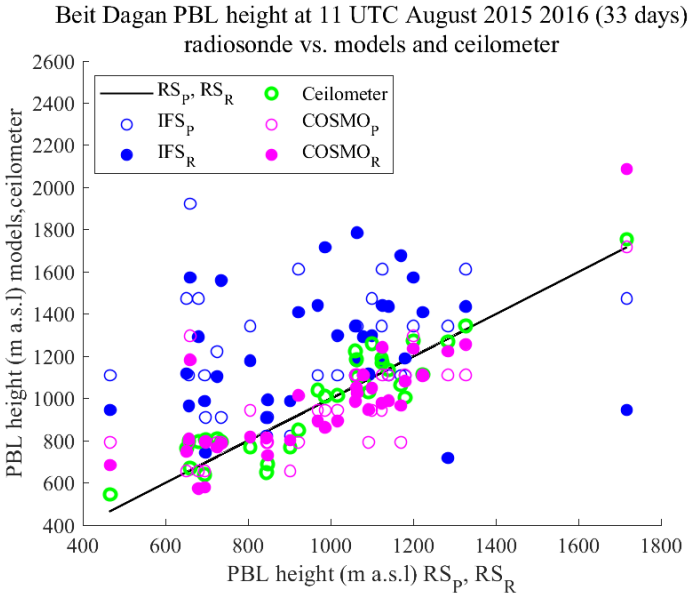

Fig 2. PBL heights over Beit Dagan site on 33 summer days (13 days on August 2015 and 20 days on August 2016), generated by the bulk Richardson method for IFS model (IFS_R, blue solid circles), COSMO model ($COSMO_R$, pink solid circles), and Beit Dagan radiosonde profiles (RS_R, black line). PBL heights generated by the parcel method for IFS model (IFS_P, open blue circles), COSMO model ($COSMO_P$, open pink circles), and Beit Dagan radiosonde profiles (RS_P, same black line as RS_R, the results are identical). PBL heights derived from the Beit Dagan ceilometer produced by the WCT method (green circles).

https://doi.org/10.5194/acp-2019-790
Preprint. Discussion started: 7 October 2019

Atmospheric Chemistry and Physics Discussions

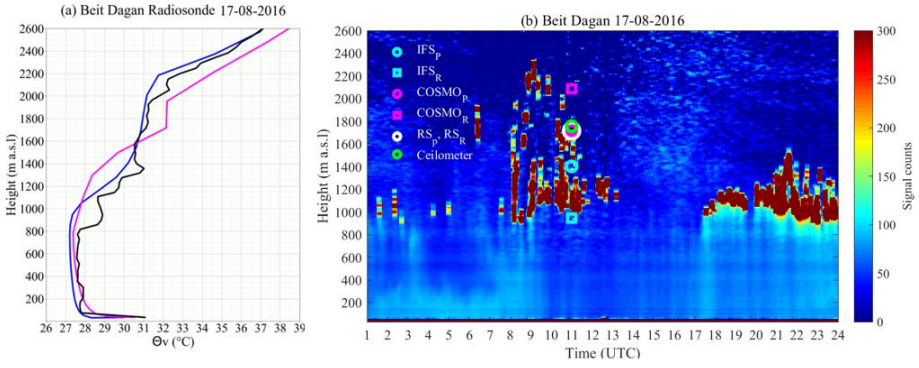

585 Fig.3 Virtual potential temperature profiles (a) from Beit Dagan radiosonde (black lines), IFS model (blue lines) and COSMO model (pink lines) and, (b) ceilometer signal counts plot on August 17, 2016 including indications of the PBL heights from the models (IFS_R, IFS_P, $COSMO_R$, $COSMO_P$), radiosonde (RS_R, RS_P) and ceilometer.

590

595

https://doi.org/10.5194/acp-2019-790
Preprint. Discussion started: 7 October 2019

Atmospheric Chemistry and Physics Discussions

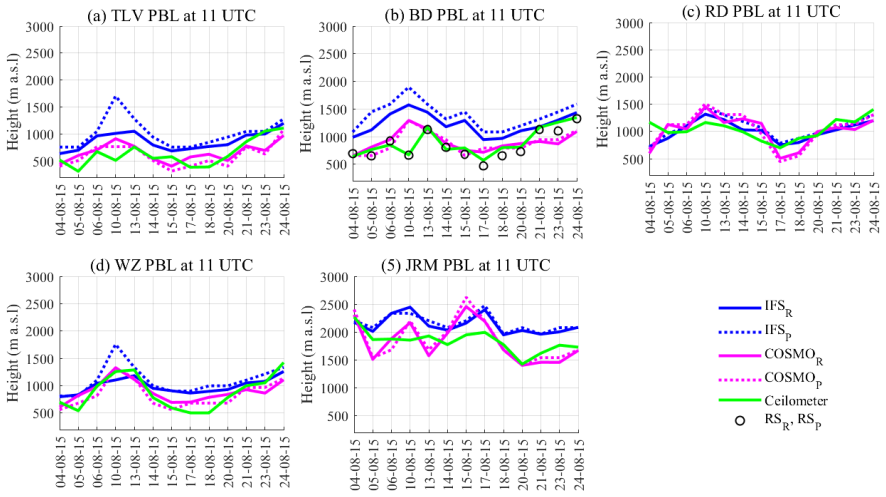

Fig. 4 PBL heights on 13 August days in 2015 from five ceilometer sites: (a) Tel Aviv (TLV), (b) Beit Dagan (BD), (c) Ramat David (RD), (d) Weizmann (WZ), and (e) Jerusalem (JRM). PBL heights were generated by the bulk Richardson method for IFS model (IFS_R, blue solid line) and the COSMO model ($COSMO_R$, pink solid line). PBL heights generated by the parcel method for IFS model (IFS_P, blue dashed line) and the COSMO model ($COSMO_P$, pink dashed line). Beit Dagan radiosonde profiles (RS_R, RS_P, black circles). PBL heights derived from the Beit Dagan ceilometer (green line) were produced by the WCT method.

https://doi.org/10.5194/acp-2019-790
Preprint. Discussion started: 7 October 2019

Atmospheric Chemistry and Physics Discussions

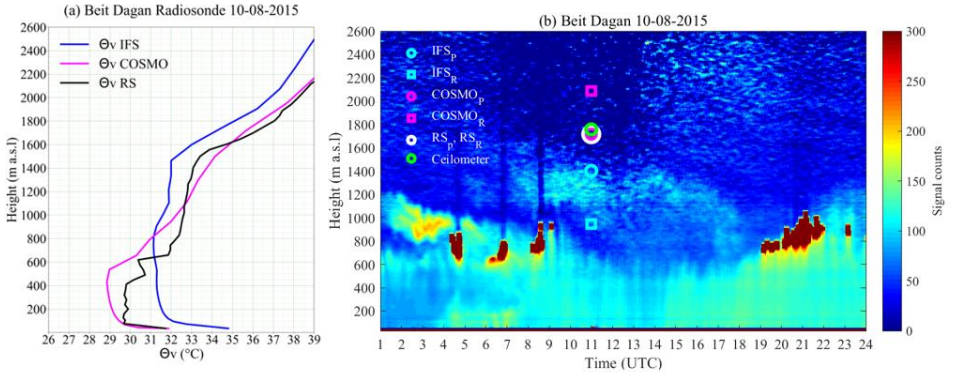

Fig.5 Virtual potential temperature profiles (a) from Beit Dagan radiosonde (black lines), IFS model (blue lines) and COSMO model (pink lines) and, (b) ceilometer signal counts plot on August 10, 2015 including indications of the PBL heights from the models (IFS_R, IFS_P, $COSMO_R$, $COSMO_P$), radiosonde (RS_R, RS_P) and ceilometer.

https://doi.org/10.5194/acp-2019-790
Preprint. Discussion started: 7 October 2019

Atmospheric Chemistry and Physics Discussions

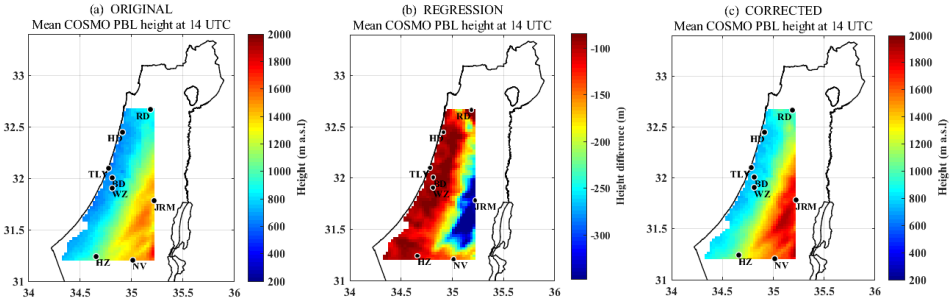

Fig. 6 Three dimensional maps of $COSMO_R$ mean PBL heights over Israel at 14 UTC before (a) and after (c) correction. The regression (b) given in Eq. (10) depicts the height difference between $COSMO_R$ and the ceilometers. The analysis was performed on the number of available days for each site on August 2015 as follows: Jerusalem - 21 days, Nevatim - 13 days, Hazerim - 20 days, Ramat David - 26 days, Weizmann - 25 days, Beit Dagan - 13 days, Hadera - 16 days, Tel Aviv - 25 days.

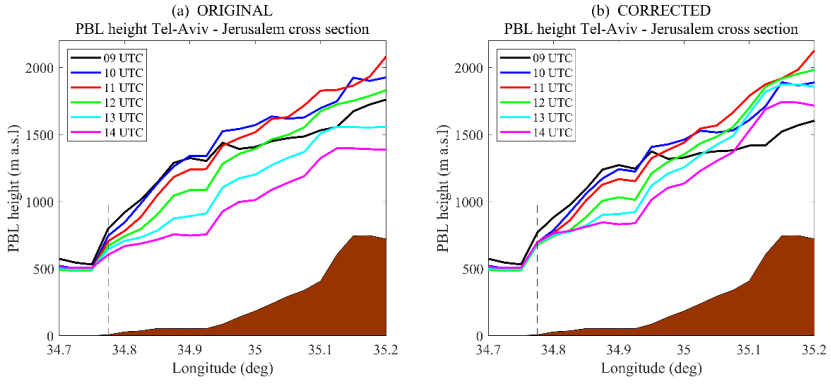

Fig. 7 $COSMO_R$ mean PBL height cross section from Tel Aviv to Jerusalem before (a) and after (b) correction between 9-14 UTC. The analysis was performed on the number of available days for each site on August 2015 as follows: Jerusalem - 21 days, Nevatim - 13 days, Hazerim - 20 days, Ramat David - 26 days, Weizmann - 25 days, Beit Dagan - 13 days, Hadera - 16 days, Tel Aviv - 25 days. The seashore (dashed line) and the topography (brown area) are also shown.